



**HAL**  
open science

## Atomic characterization of Au clusters in vapor-liquid-solid grown silicon nanowires

Wanghua Chen, Philippe Pareige, Celia Castro, Tao Xu, B. Grandidier, Didier Stiévenard, Pere Roca I Cabarrocas

### ► To cite this version:

Wanghua Chen, Philippe Pareige, Celia Castro, Tao Xu, B. Grandidier, et al.. Atomic characterization of Au clusters in vapor-liquid-solid grown silicon nanowires. *Journal of Applied Physics*, 2015, 118 (10), pp.104301. 10.1063/1.4930143 . hal-01230692

**HAL Id: hal-01230692**

**<https://polytechnique.hal.science/hal-01230692>**

Submitted on 25 May 2022

**HAL** is a multi-disciplinary open access archive for the deposit and dissemination of scientific research documents, whether they are published or not. The documents may come from teaching and research institutions in France or abroad, or from public or private research centers.

L'archive ouverte pluridisciplinaire **HAL**, est destinée au dépôt et à la diffusion de documents scientifiques de niveau recherche, publiés ou non, émanant des établissements d'enseignement et de recherche français ou étrangers, des laboratoires publics ou privés.

# Atomic characterization of Au clusters in vapor-liquid-solid grown silicon nanowires

Cite as: J. Appl. Phys. **118**, 104301 (2015); <https://doi.org/10.1063/1.4930143>

Submitted: 16 July 2015 • Accepted: 25 August 2015 • Published Online: 08 September 2015

Wanghua Chen, Philippe Pareige, Celia Castro, et al.



View Online



Export Citation



CrossMark

## ARTICLES YOU MAY BE INTERESTED IN

[Insights into gold-catalyzed plasma-assisted CVD growth of silicon nanowires](#)

Applied Physics Letters **109**, 043108 (2016); <https://doi.org/10.1063/1.4960106>

[Diameter-controlled synthesis of single-crystal silicon nanowires](#)

Applied Physics Letters **78**, 2214 (2001); <https://doi.org/10.1063/1.1363692>

[Growth-in-place deployment of in-plane silicon nanowires](#)

Applied Physics Letters **99**, 203104 (2011); <https://doi.org/10.1063/1.3659895>

Lock-in Amplifiers  
up to 600 MHz



Zurich  
Instruments



# Atomic characterization of Au clusters in vapor-liquid-solid grown silicon nanowires

Wanghua Chen,<sup>1</sup> Philippe Pareige,<sup>2</sup> Celia Castro,<sup>2</sup> Tao Xu,<sup>3</sup> Bruno Grandidier,<sup>3</sup> Didier Stiévenard,<sup>3</sup> and Pere Roca i Cabarrocas<sup>1</sup>

<sup>1</sup>Laboratoire de Physique des Interfaces et Couches Minces (LPICM), UMR 7647, CNRS, Ecole Polytechnique, 91128 Palaiseau, France

<sup>2</sup>Groupe de Physique des Matériaux (GPM), Université et INSA de Rouen, UMR 6634, CNRS, Av. de l'Université, BP 12, 76801 Saint Etienne du Rouvray, France

<sup>3</sup>Institut d'Electronique et de Microélectronique et de Nanotechnologies (IEMN), UMR 8520, CNRS, Département ISEN, 41 bd Vauban, 59046 Lille Cedex, France

(Received 16 July 2015; accepted 25 August 2015; published online 8 September 2015)

By correlating atom probe tomography with other conventional microscope techniques (scanning electron microscope, scanning transmission electron microscope, and scanning tunneling microscopy), the distribution and composition of Au clusters in individual vapor-liquid-solid grown Si nanowires is investigated. Taking advantage of the characteristics of atom probe tomography, we have developed a sample preparation method by inclining the sample at certain angle to characterize the nanowire sidewall without using focused ion beam. With three-dimensional atomic scale reconstruction, we provide direct evidence of Au clusters tending to remain on the nanowire sidewall rather than being incorporated into the Si nanowires. Based on the composition measurement of Au clusters ( $28\% \pm 1\%$ ), we have demonstrated the supersaturation of Si atoms in Au clusters, which supports the hypothesis that Au clusters are formed simultaneously during nanowire growth rather than during the cooling process.

© 2015 AIP Publishing LLC. [<http://dx.doi.org/10.1063/1.4930143>]

## I. INTRODUCTION

Investigations of metal catalysts in Si nanowires (SiNWs) have been of major interests in recent years.<sup>1-3</sup> Concerning the synthesis of SiNWs, the Chemical Vapor Deposition (CVD) via Vapor-Liquid-Solid (VLS) mechanism is widely used.<sup>4</sup> For CVD-based NW synthesis, Au is a commonly used catalyst<sup>5-8</sup> because it can provide a good control over the NW morphology due to the high surface tension of this element (1.1 N/m) and the large solubility of Si (18.6 at. %) in the liquid eutectic alloy as compared to other catalysts such as Sn (0.55 N/m and  $<10^{-8}$  at. %) and Bi (0.35 N/m and  $<10^{-4}$  at. %).<sup>9</sup> Another important advantage of Au catalyst is that Au does not oxidize when exposed to air as compared to all other metal catalyst. However, Au atoms may diffuse during NW growth,<sup>10,11</sup> which is detrimental to the electronic properties of SiNWs.<sup>12,13</sup> To understand the diffusion of Au atoms during SiNW growth, it is important to locate these Au atoms and determine their chemical environment. Several groups have shown the existence of Au clusters on the SiNW surface by High-Angle Annular Dark Field (HAADF) Scanning Transmission Electron Microscope (STEM)<sup>14</sup> and Transmission Electron Microscope (TEM).<sup>15</sup> The radius and thickness of Au clusters can be roughly obtained from their STEM or TEM results. But the composition of Au clusters has not been addressed so far. Knowing the exact composition of Au clusters can improve our understanding about this growth mechanism. Although the characterization of SiNWs has been already achieved by using Atom Probe Tomography (APT),<sup>3,6,16,17</sup> the 3D atomic mapping of Au clusters as well as their compositions are hitherto unreported. In this work,

Scanning Electron Microscope (SEM), STEM, Scanning Tunneling Microscope (STM), and APT techniques are correlated to investigate individual SiNWs. The exact composition of Au clusters has been measured besides their morphologies. As far as the APT characterization is considered, our calculation of the analyzed volume shows that the specimen sidewall information is missing during the APT characterization. To overcome this, we develop here a sample preparation method by taking advantage of the projection principle of APT.

## II. METHODS

APT being a projection microscope, the analyzed volume is directly related to the analyzed surface, which depends on the tip radius  $R$  and the working distance  $L$  between the tip and the Position Sensitive Detector (PSD). For APT reconstruction, several protocols have been designed.<sup>18,19</sup> The standard global reconstruction technique of APT is based on a protocol designed by Bas *et al.*<sup>18</sup> The calculation here is also based on this protocol. Considering the geometry of a typical specimen as illustrated in Fig. 1(a), the radius of analyzed volume  $r$  can be deduced

$$r = R \sin \theta = R \sin [(m + 1)\theta'] = R \sin \left[ (m + 1) \arctan \frac{R_D}{L} \right], \quad (1)$$

where,  $R$  is the sample radius;  $\theta$  is the angle between OA and OB (Fig. 1(a));  $\theta'$  is the angle between PA and PO (Fig. 1(a));  $m$  is a dimensionless geometric factor illustrated as PO in Fig. 1(a), which is chosen to be 0.6 in this work;  $R_D$  is the detector radius; and  $L$  is the working distance between

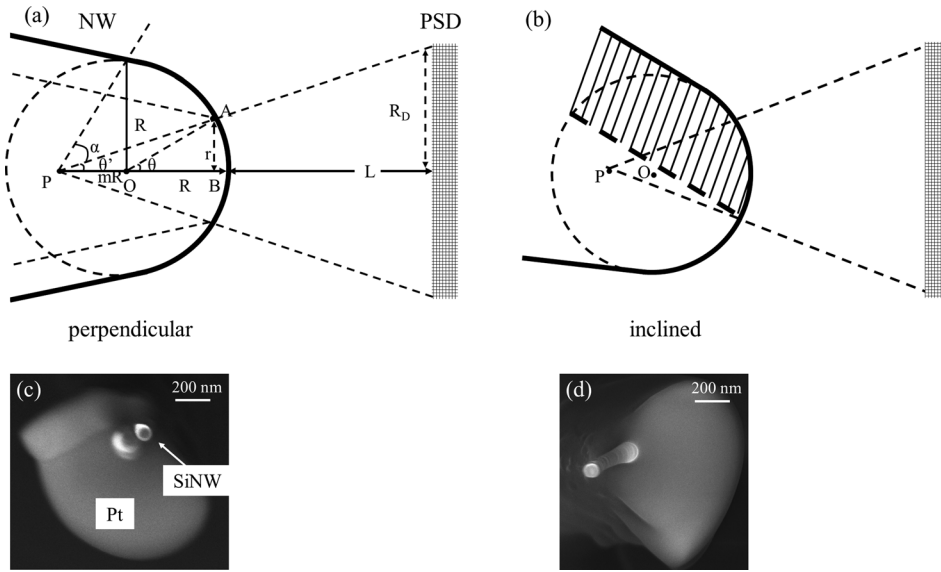


FIG. 1. Schematic illustration of projection when specimen is (a) perpendicular or (b) inclined with respect to the position sensitive detector. At a working distance  $L$  for APT with conventional configuration, the projection and analyzed volume are presented with black dot dashed line and shadow zone respectively. Top views in SEM of a specimen (NW) when the specimen tip is (c) perpendicular for STEM or (d) inclined for APT.

sample and detector. From Eq. (1), we can see that NW surface information is missing during the analysis (regardless of NW radius) when the NW is perpendicular to the APT detector. We can also see from Eq. (1) that the possibilities to have the specimen sidewall information would be to decrease the working distance  $L$  or to increase the PSD diameter. However, a decrease of the working distance will degenerate the detection limit and increasing the detector diameter once it has been set up in the analysis chamber is ruled out. The most appropriate way to obtain the surface information of the specimen is to incline it with respect to PSD as shown in Fig. 1(b). In order to collect the whole specimen sidewall surface, the minimum inclined angle can be calculated as follows:

$$\tan \alpha = \tan[(\alpha + \theta') - \theta'] = \frac{1/m - R_D/L}{1 + R_D/mL}, \quad (2)$$

where  $m$ ,  $R_D$ , and  $L$  are equal to 0.6, 3.85, and 9.8 cm, respectively. Then, the inclined angle  $\alpha$  is calculated to be  $38^\circ$ . If one wants to analyze the specimen sidewall surface, the sample inclined angle must thus be larger than  $38^\circ$  as in this work. It should be noted here that for ensuring a sufficient evaporation field on the apex surface, a specimen analyzed by the APT should have a tip diameter normally smaller than 100 nm. The properly manipulated individual SiNW in work is already an excellent specimen for APT.

In order to have a sample of inclined NW with controlled angle, a single SiNW was welded on a W support tip without the intermediate *in-situ* lift-out technique (Focused Ion Beam (FIB)). Two steps are involved in our method. The first step consists in catching a single SiNW with a W tip under an optical microscope. The second step is the welding of SiNW to the W support, thanks to Electron beam-induced deposition (EBID) mode in the Scanning Electron Microscope-Gas Injection System (SEM-GIS) manipulator workstation using Pt as the welding solder Figs. 1(c) and 1(d). The top view of the NW-tip is checked before welding. The inclination of SiNW is realized by controlling the W tip vertex angle and the welding position under SEM cross-section inspection.

Note that in our sample preparation method, neither Focused Ion Beam (FIB, contamination of Ga) nor the protection layer (Pt and W, contamination of Pt, W, and C) on the interested area of SiNWs is used as compared to the conventional FIB-based sample preparation method.<sup>20,21</sup>

SiNWs are intentionally grown at a low  $\text{SiH}_4$  pressure in order to trigger Au diffusion during NW growth. The total growth pressure is kept at 1.1 mbar and  $\text{SiH}_4$  with a flow of 12 SCCM is used to provide the Si precursors.  $\text{SiH}_4$  was further diluted in  $\text{H}_2$  as the carrier gas at a flow rate of 150 SCCM. The temperature and time of synthesis are  $500^\circ\text{C}$  and 30 min, respectively. The APT (CAMECA LaWaTAP) analyzing conditions are set at 80 K with a chamber pressure of about  $10^{-10}$  mbar. The laser is operating in the UV (343 nm) with a power of 2.8 mW. This enables an excellent evaporation rate. For the characterization of STM, an additional annealing ( $800^\circ\text{C}$  for 10 min) was performed on the same sample in order to remove the oxidation layer which can prevent the detection of the tunneling current in STM. The temperature, specimen voltage and tunneling current for acquisition of STM images are 77 K,  $-1.6$  V, and 100 pA, respectively.

### III. RESULTS

At first, the position of Au atoms on the SiNWs is investigated by conventional microscopies: SEM, STEM, and STM. Fig. 2 shows the images of these characterization techniques. In Fig. 2(a), the STEM image shows clearly the decoration of  $\langle 111 \rangle$ -oriented SiNW sidewall by Au clusters. The NW sidewall facet is also evidenced. The orientation of the (111) planes on the top sidewall is indicated. From Fig. 2(a) we can see that there is no decoration of Au cluster on  $\langle 111 \rangle$ -oriented facets. The mean radius of these Au clusters is 1.5 nm. The inset shows an SEM image of an NW where the top Au droplet and NW base are seen. Fig. 2(b) is the STM image of annealed SiNW faceted sidewall surface. Au clusters exist only on the facet with high index orientation such as  $[-1-15]$ . No decoration of Au cluster on  $\langle 111 \rangle$  sidewall facets is observed. One point should be noted here that these Au clusters have much larger mean diameters (14 nm)

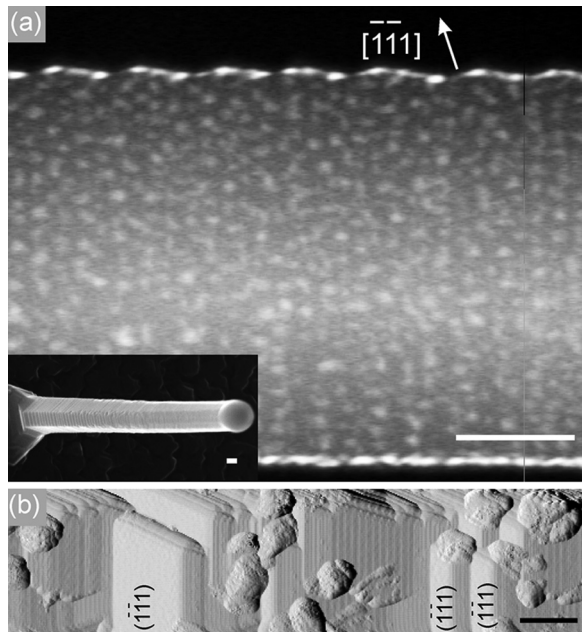


FIG. 2. (a) HAADF-STEM image of a  $\langle 111 \rangle$ -oriented SiNW, where Au clusters appear as bright protrusions decorating the high index planes of the NW faceted sidewalls. The orientation of the  $(111)$  planes on the upper sidewall is indicated. Inset: SEM image of a similar SiNW where the top Au seed droplet and the base of the NW are seen. (b) STM image of an NW sidewall showing the Au clusters self-assembled on the high index planes, which alternate with  $(111)$  plane. The widest  $(111)$  planes are labelled. The scale bars correspond to 20 nm.

as compared to the one without annealing. This can be explained by the Ostwald ripening during the heating process.

APT which is a 3D atomic resolution technique is used to probe atomic species and their location in the NWs. By taking the advantage of APT, different elements in individual SiNWs are detected and viewed in 3D space. Fig. 3(a) shows the mass-to-charge spectrum of a SiNW grown via VLS mechanism using Au as metal catalyst. The Si isotopes have several peaks both at one charge and two charges. The H isotopes have also been detected due to the interaction between background gas H and the tip. Fig. 3(b) is 3D reconstruction of an individual SiNW using the sample preparation method described previously by inclination of SiNW with a slice of atomic resolved reconstruction showing Au cluster decoration on Si facet and Si  $(111)$  planes normal to NW growth direction. Au atoms can be clearly seen at the NW surface, while the Au concentration in SiNW core is below our detection level of  $3 \times 10^{17}$  Au/cm<sup>3</sup>. Such low incorporation of Au atoms into SiNWs during NW growth is expected because of the low equilibrium solubility of Au in Si (e.g.,  $2 \times 10^{15}$  Au/cm<sup>3</sup> in Si at 650 °C).<sup>22</sup> As it can be seen in the reconstruction of Fig. 3(b), Au atoms tend to form clusters on SiNW sidewalls, rather than being homogeneously distributed. It has been presented and discussed in our previous study that at low growth pressure the migration of Au atoms from the seed particle and the lateral NW growth take place at the same time<sup>23,24</sup> which could imply a partial embedding of the Au clusters into the volume of the Si NWs. However, Fig. 3(b) clearly shows that Au atoms prefer to

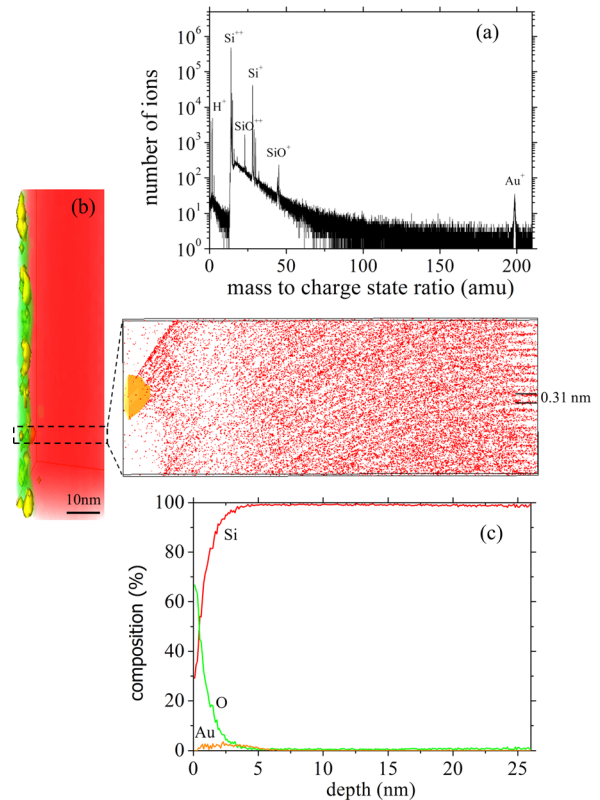


FIG. 3. (a) Mass-to-charge spectrum of Au-catalyzed VLS-grown SiNWs. (b) Atomically resolved reconstruction of an individual SiNW with a slice of atomic resolved reconstruction showing Au cluster decoration on Si facet and Si  $(111)$  planes normal to NW growth direction with inter plane distance of  $0.31 \pm 0.01$  nm. Si, Au, and O atoms are represented by red, yellow, and green, respectively. (c) Distribution of Si, Au, and O atom composition along the cross-section of individual SiNW.

“float” on SiNW sidewall rather than penetrate into SiNW. The reason is that the chemical potential of Au atoms in the SiNW bulk is higher than on SiNW sidewall.<sup>25</sup> We also observe in Fig. 3(b) that the Au clusters, which are surrounded by the Si native oxide layer, are not completely buried in this layer. Note that in Fig. 3(b) some Au clusters are surrounded by a native Si oxide layer due to the 3D view of NW sidewall. From Fig. 3(b), we find a mean radius and thickness for the clusters of 4 nm and 3 nm, respectively. The identification of Au clusters is done based on the raw APT data using the so-called INN statistical method.<sup>26</sup> The composition of Si atoms in the Au cluster is calculated to be  $28\% \pm 1\%$ . This value is larger than the one in the bulk liquid Au-Si alloy showing that the Si composition in nanoscale clusters increases. Sutter *et al.* calculated the Si composition of 26% in Au-Si droplet (radius: 4 nm) based on the capillarity and surface stress.<sup>27,28</sup> A composition profile along the cross-section was also made to analyze quantitatively the interface between the Au cluster/SiO<sub>x</sub> and SiNWs by moving a slice with a 1 nm step along the axis of cross-section (Fig. 3(c)). The composition of the outer layer is calculated to be: Si: 28.3%, O: 65.2% which is near the stoichiometry of SiO<sub>2</sub>. From Fig. 3(c), we can see that there is a 5 nm-thick transition layer between SiO<sub>2</sub> layer and SiNW. There is a gradual decrease of O content and an increase of Si content in SiO<sub>x</sub> layer up to 5 nm from the surface. A similar

transition layer across Si-SiO<sub>2</sub> interface has been reported by Batson *at al.*, using electron energy-loss spectroscopy (EELS) technique.<sup>29</sup>

The literature suggests that the Au clusters are formed as pure solid Au clusters from the liquid thin Au/Si film when NWs are cooled to room temperature after NW growth.<sup>30</sup> However, in this work, the higher concentration of Si in Au clusters strongly indicates that they are formed simultaneously during NW growth. We think that the increase of Si concentration in Au clusters is rather due to the supersaturation of Si atoms in clusters which are also exposed to silane during SiNW growth. As the Au clusters are formed during NW growth (bonded directly on NW sidewall), Si nano-branches grown on the trunk of SiNW could be catalyzed simultaneously in one step under fixed conditions as observed in the literature.<sup>31</sup>

#### IV. CONCLUSIONS

In summary, multi-techniques, namely, SEM, STEM, STM, and APT have been applied to investigate the localized position of Au atoms in an individual SiNW. The existence of nano clusters on SiNW sidewall surface is clearly evidenced. We have developed a method to analyze NW sidewall surface. Using this method, NW is welded intentionally on support tip with an inclination for APT. The combination of these techniques allows us to show that Au atoms diffuse from the seed particle at the top of the NW and form Au clusters on the NW sidewalls but do not penetrate inside the NW (the Au concentration in the SiNW interior is measured to be below  $3 \times 10^{17}$  Au/cm<sup>3</sup>). The composition of Si in these nano clusters is measured to be  $28\% \pm 1\%$  which is larger than the estimation from phase diagram due to the supersaturation of Si atoms.

<sup>1</sup>O. Moutanabbir, D. Isheim, H. Blumtritt, S. Senz, E. Pippel, and D. N. Seidman, *Nature* **496**, 78 (2013).

<sup>2</sup>H. Wang, L. A. Zepeda-Ruiz, G. H. Gilmer, and M. Upmanyu, *Nat. Commun.* **4**, 1956 (2013).

<sup>3</sup>W. Chen, L. Yu, S. Misra, Z. Fan, P. Pareige, G. Patriarche, S. Bouchoule, and P. Roca i Cabarrocas, *Nat. Commun.* **5**, 4134 (2014).

<sup>4</sup>R. S. Wagner and W. C. Ellis, *Appl. Phys. Lett.* **4**, 89 (1964).

<sup>5</sup>H. Yan, H. S. Choe, S. Nam, Y. Hu, S. Das, J. F. Klemic, J. C. Ellenbogen, and C. M. Lieber, *Nature* **470**, 240 (2011).

<sup>6</sup>W. Chen, V. G. Dubrovskii, X. Liu, T. Xu, R. Larde, J. P. Nys, B. Grandidier, D. Stievenard, G. Patriarche, and P. Pareige, *J. Appl. Phys.* **111**, 094909 (2012).

<sup>7</sup>M. M. Gabriel, J. R. Kirschbrown, J. D. Christesen, C. W. Pinion, D. F. Zigler, E. M. Grumstrup, B. P. Mehl, E. E. M. Cating, J. F. Cahoon, and J. M. Papanikolas, *Nano Lett.* **13**, 1336 (2013).

<sup>8</sup>N. Gao, W. Zhou, X. Jiang, G. Hong, T.-M. Fu, and C. M. Lieber, *Nano Lett.* **15**, 2143 (2015).

<sup>9</sup>H. Baker and H. Okamoto, *ASM Handbook, Volume 3-Alloy Phase Diagrams* (ASM International, 1992).

<sup>10</sup>J. B. Hannon, S. Kodambaka, F. M. Ross, and R. M. Tromp, *Nature* **440**, 69 (2006).

<sup>11</sup>M. Bar-Sadan, J. Barthel, H. Shtrikman, and L. Houben, *Nano Lett.* **12**, 2352 (2012).

<sup>12</sup>A. J. Tavendale and S. J. Pearton, *J. Phys. C: Solid State Phys.* **16**, 1665 (1983).

<sup>13</sup>E. Koren, G. Elias, A. Boag, E. R. Hemesath, L. J. Lauhon, and Y. Rosenwaks, *Nano Lett.* **11**, 2499 (2011).

<sup>14</sup>G.-S. Park, H. Kwon, D. W. Kwak, S. Y. Park, M. Kim, J.-H. Lee, H. Han, S. Heo, X. S. Li, J. H. Lee, Y. H. Kim, J.-G. Lee, W. Yang, H. Y. Cho, S. K. Kim, and K. Kim, *Nano Lett.* **12**, 1638 (2012).

<sup>15</sup>D.-W. Seo, G.-S. Kim, C.-Y. Lee, S.-Y. Lee, J.-H. Hyung, C.-J. Choi, and S.-K. Lee, *J. Appl. Phys.* **111**, 034301 (2012).

<sup>16</sup>J. E. Allen, E. R. Hemesath, D. E. Perea, J. L. Lensch-Falk, Z. Y. Li, F. Yin, M. H. Gass, P. Wang, A. L. Bleloch, R. E. Palmer, and L. J. Lauhon, *Nat. Nanotechnol.* **3**, 168 (2008).

<sup>17</sup>J. G. Connell, K. Yoon, D. E. Perea, E. J. Schwalbach, P. W. Voorhees, and L. J. Lauhon, *Nano Lett.* **13**, 199 (2013).

<sup>18</sup>P. Bas, A. Bostel, B. Deconihout, and D. Blavette, *Appl. Surf. Sci.* **87-88**, 298 (1995).

<sup>19</sup>B. P. Geiser, D. J. Larson, E. Oltman, S. Gerstl, D. Reinhard, T. F. Kelly, and T. J. Prosa, *Microsc. Microanal.* **15**, 292 (2009).

<sup>20</sup>P. D. Cherns, F. Lorut, C. Dupré, K. Tachi, D. Cooper, A. Chabli, and T. Ernst, *J. Phys.: Conf. Ser.* **209**, 012046 (2010).

<sup>21</sup>M. El Kousseifi, F. Panciera, K. Hoummada, M. Descoins, T. Baron, and D. Manginck, *Microelectron. Eng.* **120**, 47 (2014).

<sup>22</sup>C. B. Collins, R. O. Carlson, and C. J. Gallagher, *Phys. Rev.* **105**, 1168 (1957).

<sup>23</sup>W. Chen, R. Larde, E. Cadel, T. Xu, B. Grandidier, J. P. Nys, D. Stievenard, and P. Pareige, *J. Appl. Phys.* **107**, 084902 (2010).

<sup>24</sup>T. Xu, J. P. Nys, A. Addad, O. I. Lebedev, A. Urbietta, B. Salhi, M. Berthe, B. Grandidier, and D. Stievenard, *Phys. Rev. B* **81**, 115403 (2010).

<sup>25</sup>M. I. den Hertog, J.-L. Rouviere, F. Dhalluin, P. J. Desré, P. Gentile, P. Ferret, F. Oehler, and T. Baron, *Nano Lett.* **8**, 1544 (2008).

<sup>26</sup>T. Philippe, F. De Geuser, S. Duguay, W. Lefebvre, O. Cojocar-Mirédin, G. Da Costa, and D. Blavette, *Ultramicroscopy* **109**, 1304 (2009).

<sup>27</sup>E. J. Schwalbach and P. W. Voorhees, *Nano Lett.* **8**, 3739 (2008).

<sup>28</sup>E. Sutter and P. Sutter, *Nano Lett.* **8**, 411 (2008).

<sup>29</sup>P. E. Batson, *Nature* **366**, 727 (1993).

<sup>30</sup>P. Madras, E. Dailey, and J. Drucker, *Nano Lett.* **10**, 1759 (2010).

<sup>31</sup>T. Kawashima, T. Mizutani, T. Nakagawa, H. Torii, T. Saitoh, K. Komori, and M. Fujii, *Nano Lett.* **8**, 362 (2008).